Journal of Materials Science and Engineering B 14 (1-3) (2024) 14-20
doi: 10.17265/2161-6221/2024.1-3.003

First-Principle Study on the Electronic Structure and Optical Property of New Diluted Magnetic Semiconductor $(Y_{0.75}Ca_{0.25})(Cu_{0.75}Mn_{0.25})SO$

Zhou Wenjie

College of Science, Jiliang University, Hangzhou 310018, China

Abstract: The band structure, DOSs, and optical properties of $(Y_{0.75}Ca_{0.25})(Cu_{0.75}Mn_{0.25})SO$, including dielectric function, absorption function, reflection function, and energy loss spectrum were studied by using the first-principles calculation. The calculation results indicate that $(Y_{0.75}Ca_{0.25})(Cu_{0.75}Mn_{0.25})SO$ is a direct bandgap semiconductor with a bandgap of 1.1 eV. The Fermi surface is asymmetric and exhibits spin splitting phenomenon. The new type of dilute magnetic semiconductor $(Y_{0.75}Ca_{0.25})(Cu_{0.75}Mn_{0.25})SO$ exhibits significant light loss around 70 eV, with light reflection gradually increasing after 30 eV, and light absorption mainly occurring around 8-30 eV. These results also provide a basis for the discovery of more types of 1111 phase new dilute magnetic semiconductors in the future.

Key words: First-principles calculation, electronic structure, optical property, new diluted magnetic semiconductor.

1. Introduction

In today's rapid development in the field of nanotechnology, new diluted magnetic semiconductors have attracted widespread attention. With their unique magnetic and semiconducting properties, this class of materials offers great potential for the development of next-generation electronic devices and information storage technologies [1-6]. The study of dilute magnetic semiconductors has become a hotspot in the fields of materials science and condensed matter physics, in which new discoveries have not only pushed forward the progress of basic science, but also laid the foundation for future technological innovations. The unique properties of dilute magnetic semiconductors have made them the focus of research in many fields. These materials possess both the tunable conductivity of conventional semiconductors and exhibit very interesting spin properties, offering new possibilities for realizing spintronic devices. In addition, diluted magnetic semiconductors show promising applications in magnetic storage, quantum computing and optoelectronic conversion [7-11].

According to the molecular formula and crystal structure, new diluted magnetic semiconductors with charge and spin separation regulation have been developed into three types: 111-type, 122-type, and 1111-type. New diluted magnetic semiconductors such as Li(Zn,Mn)P, Li(Zn,Mn)As, (La,Ca)(Zn,Mn)SbO, (Ba,K)F(Zn,Mn)As, (Ba,Na)F (Zn,Mn)S, etc. have been synthesized [12, 13]. In addition to synthesizing samples, the study of dilute magnetic semiconductors involves experimental measurements and theoretical calculations, and so far there are very few articles on first-principles studies of new dilute magnetic semiconductors. We will discuss in detail the electronic structure and optical properties of selected new diluted magnetic semiconductors with a view to providing new insights and directions for research in this field. Through this research, we

Corresponding author: Wenjie Zhou, M.D., research fields: materials physics, semiconductor materials and magnetic materials.

hope to contribute to the future development of nanoelectronics and information technology. In this paper, the electronic structure and optical properties of $(Y_{0.75}Ca_{0.25})(Cu_{0.75}Mn_{0.25})SO$ are investigated by first-principles calculations.

2. Calculation Method and Theoretical Model

2.1 Calculation Method

Based on density functional theory, the generalized gradient approximation (PBE-GGA) is used in our calculations and is implemented in the VASP (Vienna Ab-initio Simulation Package) software [14]. For the calculation, the modeling of $(Y_{0.75}Ca_{0.25})(Cu_{0.75}Mn_{0.25})SO$ was first obtained through Material studio. Afterwards, the model is structurally optimized to obtain the model structure with the lowest energy, i.e. the most stable model structure. The model is used as a basis for subsequent calculations of properties such as electronic structure and optical properties. The parameters are set as follows: plane wave cutoff energy is set to 340 eV, energy convergence is set to 2×10^{-5}, and force convergence is set to 2×10^{-3}, the maximum convergence displacement of atoms is standardized to 0.001, and the calculations are carried out in the inverse easy K-space.

2.2 Theoretical Model

In order to calculate the electronic structure of $(Y_{0.75}Ca_{0.25})(Cu_{0.75}Mn_{0.25})SO$ and to study its optical properties, we constructed $2 \times 1 \times 1$ supercells [15-17]. The supercell has 16 atoms, including 4 atoms each of Y, Cu, S, and O. When we replace the S atoms with Mn atoms and at the same time replace the Y atoms with Ca atoms, we obtain the structure of $(Y_{0.75}Ca_{0.25})(Cu_{0.75}Mn_{0.25})SO$, in which the doping amounts of Mn and Ca are 0.25. As shown in Fig. 1, for simplicity there are 4 doping scenarios for Ca atoms, if we fix the Mn atoms (denoted by the purple balls). We calculated the energy of the whole supercell for each of the 4 doping cases and found that the Ca atom has the lowest energy of the whole supercell at position 3 (about -109.77683 eV), and therefore used the 3rd model for the back calculation [18].

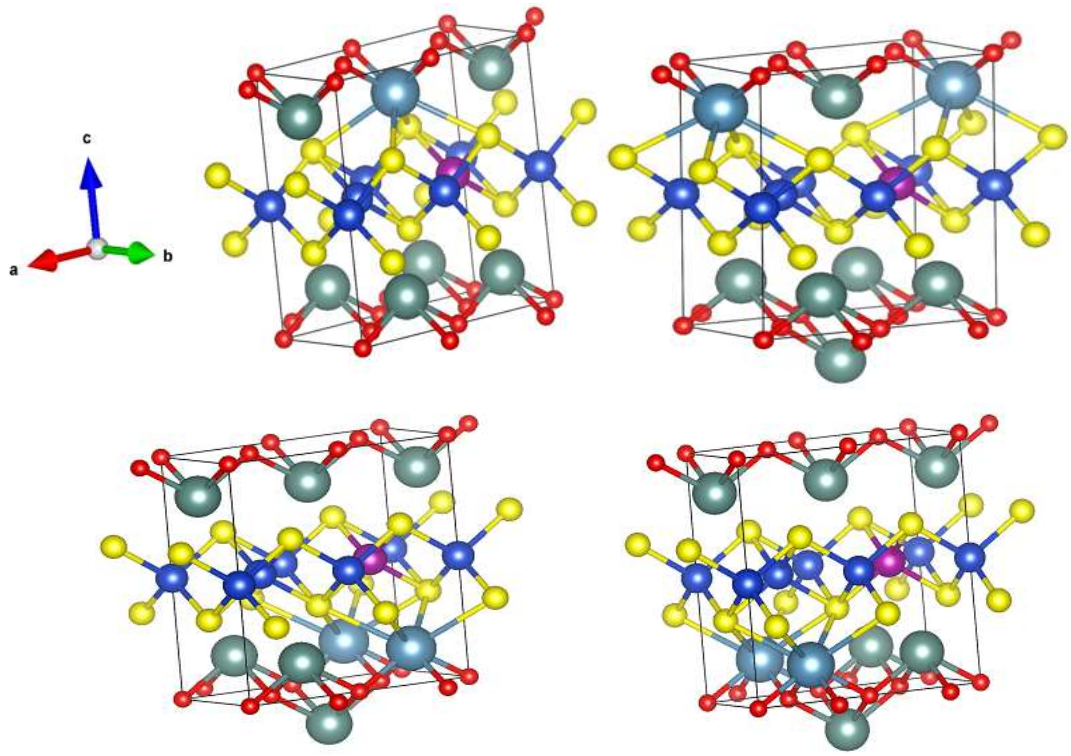

Fig. 1 The crystal structure of $(Y_{0.75}Ca_{0.25})(Cu_{0.75}Mn_{0.25})SO$.

3. Electronic Structure

The spin-up and spin-down energy band diagrams of $(Y_{0.75}Ca_{0.25})(Cu_{0.75}Mn_{0.25})SO$ are shown in Fig. 2, in which the red and black curves represent the energy band diagrams when the energy bands are in spin-up and spin-down, respectively. In both energy band diagrams, the valence band top and the conduction band bottom appear at the high symmetry point γ point in the Brillouin zone. Therefore, $(Y_{0.75}Ca_{0.25})(Cu_{0.75}Mn_{0.25})SO$ belongs to the direct bandgap semiconductors. For the spin-down region, the conduction band bottom is tangent to the Fermi surface and the valence band top is located at -1.1 eV. On the contrary, in the spin-up energy band structure, the conduction band bottom is located at 0.03 V while the valence band top is located at -0.9 eV, and the spin-down energy band gap is about 1.2 eV [19-21]. Considering the spin, the general case is that in the spin-down state, the energy levels around the Fermi surface move downward, resulting in a decrease in the band gap.

4. Electronic DOSs (Density of States)

The total electronic DOS diagram of $(Y_{0.75}Ca_{0.25})(Cu_{0.75}Mn_{0.25})SO$ is shown in Fig. 3, and the spin up and spin down are not the same, especially between 0-1 eV, where there is a more pronounced up-down asymmetry. This may be due to the doping of Mn element which brings spin to the system and the occurrence of spin cleavage.

Combined with the DOS and energy band structure, $(Y_{0.75}Ca_{0.25})(Cu_{0.75}Mn_{0.25})SO$ behaves as a dilute magnetic semiconductor.

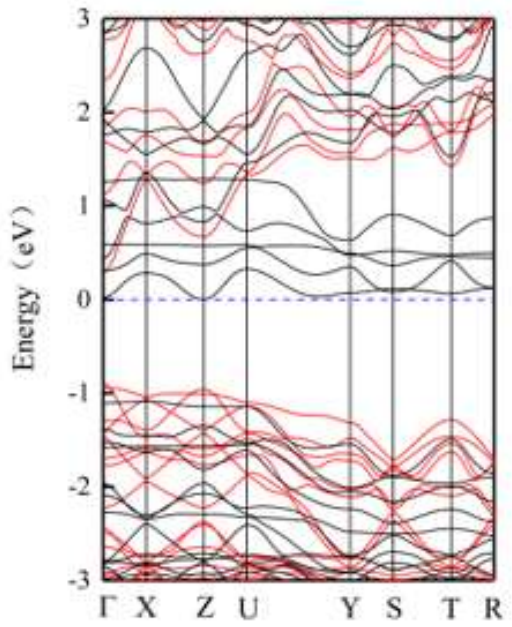

Fig. 2 Energy band structure of $(Y_{0.75}Ca_{0.25})(Cu_{0.75}Mn_{0.25})SO$.

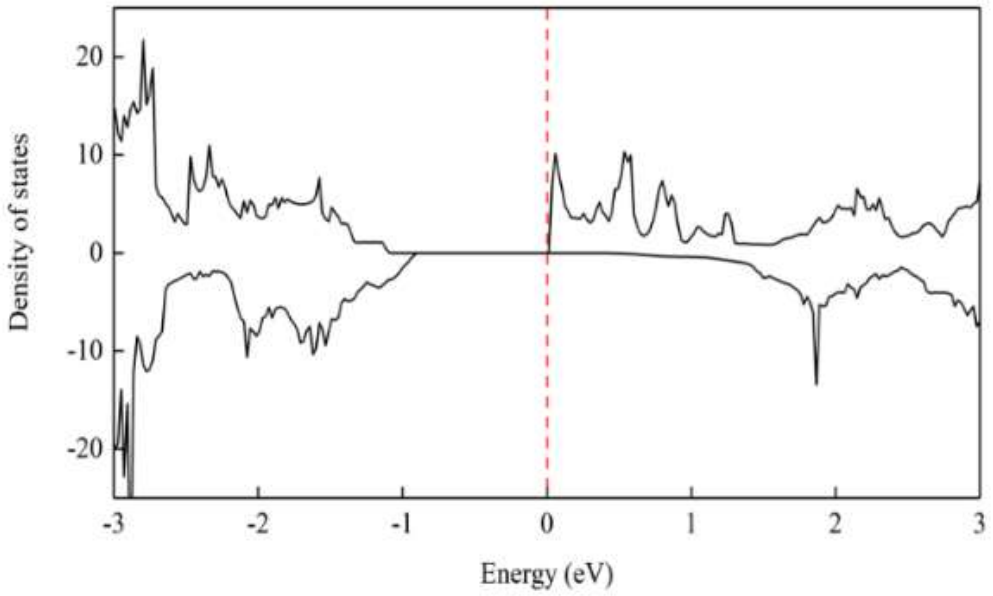

Fig. 3 Densities of $(Y_{0.75}Ca_{0.25})(Cu_{0.75}Mn_{0.25})SO$.

5. Optical Properties

5.1 Dielectric Function

In the study of diluted magnetic semiconductors, the role of first-principles calculations in exploring optical properties such as dielectric function, absorption function, reflection coefficient is gradually coming to the fore. A comparison of the curves of the real and imaginary parts of the dielectric number as a function of energy is presented in Fig. 4. It is observed that the dielectric function curves show significant differences when the incident light is oriented along the 001, 010, and 100 axes, respectively.

Consequently, the optical properties will also be anisotropic in all directions, although the difference is not significant. Therefore, the subsequent discussion will not analyze the optical properties along each axis direction in detail [22]. The static dielectric function is the real part of the dielectric function when the frequency is 0. Therefore, when the incident light is along the directions a, b and c, the values of the static dielectric function are 6.9, 7.2 and 6.8, respectively.

From the imaginary part of the dielectric function in Fig. 4, it can be observed that the dielectric function in the range of 0-5 eV shows an upward trend reaching a maximum near 6 eV with a peak of about 9. There are roughly five peaks in the imaginary part of the dielectric function curve of the figure that are more pronounced, with the highest peak between 2 eV and 10 eV, which may be attributed to the effect of the jump between the conduction and valence bands within the electronic structure.

5.2 Absorption Spectrum

The dielectric function determines the optical properties of a crystal, and there is a close relationship between the absorption function and electron jump. When light strikes the surface of a material, photons of it are absorbed by the material, causing electrons in the material to jump from the ground state of an atom or molecule to an excited state. These electron leaps lead to the absorption of light by the material, thus characterizing the absorption function. From the graph of absorption coefficient versus energy, it can be seen that the peaks are roughly divided into 4 parts, and the 2 more obvious peaks are peak 1.5×10^6 cm^{-1} near 6 eV and the peak 1.5×10^6 cm^{-1} near 9 eV which are closer to each other. By observing the intensity of the peaks, it can be found that in the high-energy part, i.e., energy between 25-30 eV, light irradiation is more likely to cause the energy level jump of electrons to occur when the substance absorbs it.

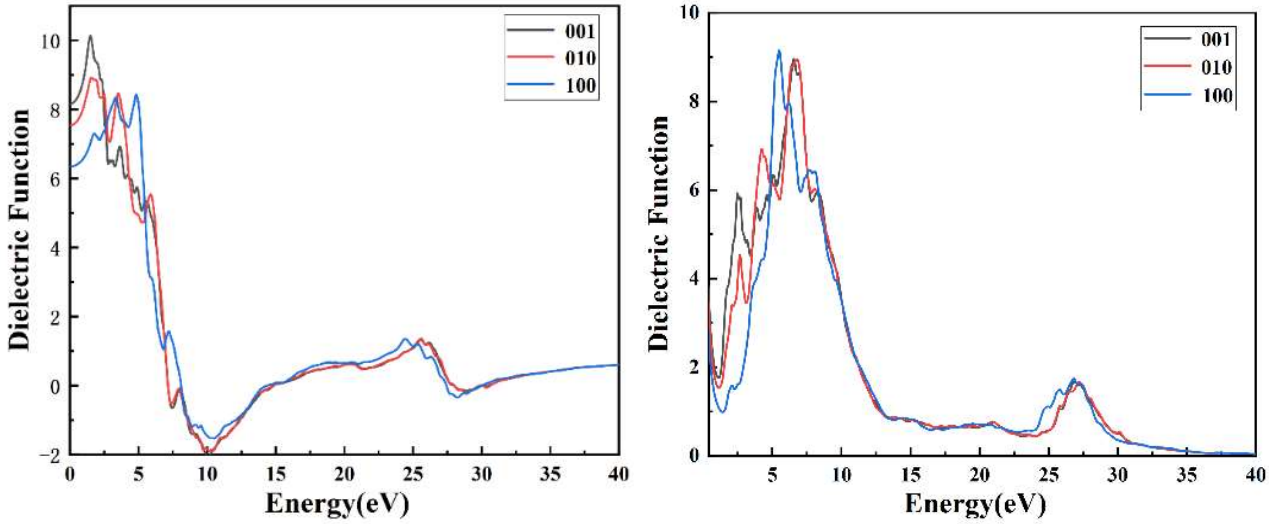

(a) Real part of the dielectric function

(b) Imaginary part of the dielectric function

Fig. 4 Dielectric function of $(Y_{0.75}Ca_{0.25})(Cu_{0.75}Mn_{0.25})SO$.

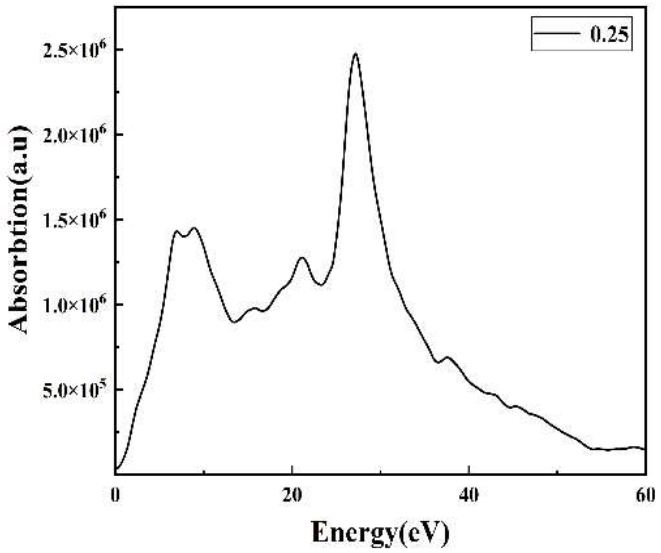

Fig. 5 Absorption spectrum of $(Y_{0.75}Ca_{0.25})(Cu_{0.75}Mn_{0.25})SO$.

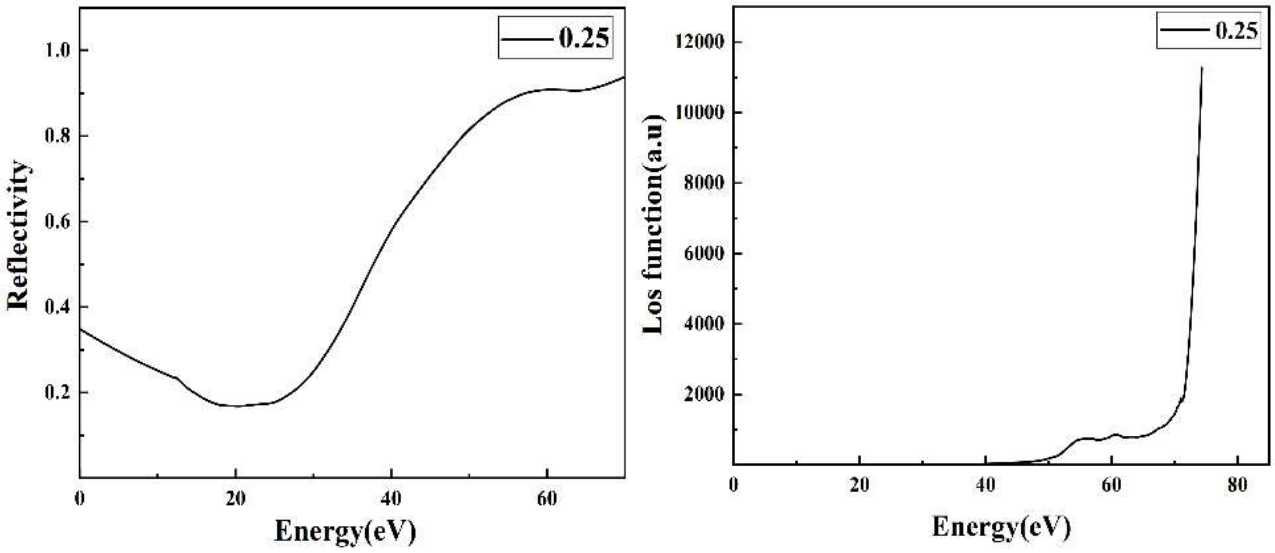

(a) Reflectivity spectrum (b) Energy-loss function

Fig. 6 Energy-loss function spectrum and reflectivity spectrum of $(Y_{0.75}Ca_{0.25})(Cu_{0.75}Mn_{0.25})SO$.

5.3 Energy-Loss Function Spectrum and Reflectivity Spectrum

In optical properties, the energy loss spectrum is commonly used to study the energy lost by a material when it is excited by a photon. From the variation of reflectance with energy in Fig. 5, it can be found that the maximum reflectance of 0.8 is located around 50 eV in the curve of its reflectance with energy, and there is a distinct subpeak near 8 eV with a size of about 0.4. Between 10 and 30 eV, the reflected intensity is stable around 0.2, the peak exists only in the UV band and the energy loss is maximum in the UV band under the photo-quantum effect. From the energy loss curves in Fig. 6, it can be found that the energy loss value peaks near 70 eV, while the rest of the position tends to level off to almost zero. The energy loss peak has a certain relationship with the loss energy range, the sharper the peak, the narrower the range, so that the crystal can reduce the energy loss, effectively increasing the crystal optical storage efficiency [23].

6. Conclusion

We have investigated the electronic structure and optical properties of ($Y_{0.75}Ca_{0.25}$)($Cu_{0.75}Mn_{0.25}$)SO using density functional theory under the generalised gradient approximation. The conclusions of the study are presented below:

(1) ($Y_{0.75}Ca_{0.25}$)($Cu_{0.75}Mn_{0.25}$)SO is a direct bandgap semiconductor with a bandgap width of about 1.1 eV and due to the introduction of Mn ions, which leads to spin cleavage and produces spin-up and spin-down asymmetries near the Fermi surface.

(2) ($Y_{0.75}Ca_{0.25}$)($Cu_{0.75}Mn_{0.25}$)SO crystals show a rather unusual finding in terms of optical properties, combining energy loss spectra and reflection curves, where the light loss is very pronounced around 70 eV, while from the absorption curves it can be found that the light absorption occurs in the range of 8-30 eV.

These results provide guidance for the experimental synthesis of novel dilute magnetic semi-providing conductors ($Y_{0.75}Ca_{0.25}$)($Cu_{0.75}Mn_{0.25}$)SO regulated by spin and charge separation.

References

[1] Wei, D. 2023. "The Room Temperature Ferromagnetism in Highly Strained Two-Dimensional Magnetic Semiconductors." *Journal of Semiconductors* 44 (4): 2. doi: 10.1088/16744926/44/4/040401.

[2] Özdoğan, K., Şaşıoğlu, E., and Galanakis, I. 2018. "Robustness and Stability of Half-Metallic Ferromagnetism in Alkaline-Earth Metal Mononitrides against Doping and Deformation." *Journal of Applied Physics* 111 (11): 113918. doi: 10.1103/RevModPhys.76.323.

[3] Li, Y., Chen, T., Ye, Y., Ding, S. B., and Wu, Z. M. 2021. "Research Progress of Magnetoelectric Properties of I-Ⅱ-V Group-Based Novel Diluted Magnetic Semiconductor." *Journal of Functional Materials* 52 (2): 2057-2065. doi: 10.3969/j.issn.1001-9731.2021.02.008.

[4] Peng, Y., Zhao, G. Q., Deng, Z., and Jin, C. Q. 2024. "Recent Advances in Application-Oriented New Generation Diluted Magnetic Semiconductors." *Acta Physica Sinica* 73 (1): 15-28.

[5] Zhao, X., Dong, J., Fu, L., Gu, Y., Zhang, R., Yang, Q., Xie, L., Tang, Y., and Ning, F. 2022. "($Ba_{1-x}Na_x$)F($Zn_{1-x}Mn_x$)Sb: A Novel Fluoride-Antimonide Magnetic Semiconductor with Decoupled Charge and Spin Doping." *Journal of Semiconductors* 43 (11): 112501.

[6] Zhao, J. H., Deng, J. J., and Zheng, H.Z. 2007. "Diluted Magnetic Semiconductors." *Progress in Physics* 27 (2): 109-50. doi: CNKI:SUN:WLXJ.0.2007-02-000.

[7] Deng, Z., Zhao, G. Q., and Jin, C. Q. 2019. "Recent Progress of a New Type Diluted Magnetic Semiconductors with Independent Charge and Spin Doping." *Acta Physica Sinica* 68 (16): 252-63. doi: CNKI:SUN:WLXB.0.2019-16-007.

[8] Hirohata, A., Sukegawa, H., Yanagihara, H., Zutic, I., Seki, T., Mizukami, S., and Swaminathan, R. 2015. "Roadmap for Emerging Materials for Spintronic Device Applications." *IEEE Transactions on Magnetics* 51 (10): 1-11. doi:10.1109/TMAG.2015.2457393.

[9] Han, W., Zhao, K., Wang, X. C., Liu, Q. Q., Ning, F. L., Deng, Z., Liu, Y., Zhu, J. L., Ding, C., Man, H. Y., and Jin, C. Q. 2013. "Diluted Ferromagnetic Semiconductor (LaCa)(ZnMn)SbO Isostructural to '1111' Type Iron Pnictide Superconductors." *Science China (Physics, Mechanics & Astronomy)* 56 (11): 2026-30.

[10] Zhao, K., Chen, B. J., Deng, Z., Han, W., Zhao, G. Q., Zhu, J. L., et al. 2014. "(Ca,Na)($Zn,Mn)_2As_2$: A New Spin and Charge Doping Decoupled Diluted Ferromagnetic Semiconductor." *Journal of Applied Physics* 116 (16): 163906. doi: 10.1063/1.4899190.

[11] Yang, J., Luo, S., Cheng, Z., Wang, X., Xiong, Y., and Amel, L. 2016. "Electronic Structures and Magnetic Properties of a II-II-V Based Diluted Magnetic Semiconductor $Ba_{1-x}K_x(Cd_{1-y}Mn_y)_2As_2$ with Decoupled Charge and Spin Doping." *Materials Research Express* 3 (10): 105903. doi: 10.1088/2053-1591/3/10/105903.

[12] Zhao, X., Dong, J., Fu, L., Gu, Y. L., Zhang, R. F., Yang, Q. L., Xie, L. F., Tang, Y. S., and Ning, F. L. 2022. "($Ba_{1-x}Na_x$)F($Zn_{1-x}Mn_x$)Sb: A Novel Fluoride-Antimonide Magnetic Semiconductor with Decoupled Charge and Spin Doping." *Journal of Semiconductors* 43 (11): 112501.

[13] Yu, S., Peng, Y., Zhao, G., Zhao, J., Wang, X., Zhang, J., Deng, Z., and Jin, C. 2023. "Colossal Negative Magnetoresistance in Spin Glass Na(Zn,Mn)Sb." *Journal of Semiconductors* 44 (3): 66-71.

[14] Peng, Y., Yu, S., Zhao, G. Q., Li, W. M., Zhao, J. F., Cao, L. P., Wang, X. C., Liu, Q. Q., Zhang, S. J., and Yu, R. Z. 2019. "Effects of Chemical Pressure on Diluted Magnetic Semiconductor (Ba,K)($Zn,Mn)_2As_2$." *Chinese Physics B* 28 (5): 057501. doi: 10.1088/1674-1056/28/5/057501.

[15] Zhao, K., Chen, B., Zhao, G., Yuan, Z., Liu, Q., Deng, Z., Zhu, J., and Jin, C. 2014. "Ferromagnetism at 230 K in ($Ba_{0.7}K_{0.3}$)($Zn_{0.85}Mn_{0.15}$)$_2As_2$ Diluted Magnetic Semiconductor." *Chinese Science Bulletin* 59 (21): 2524-7. doi: 10.1007/s11434-014-0398-z.

[16] Uti, I., and Zhou, T. 2018. "Tailoring Magnetism in

Semiconductors." *Science China Physics Mechanics & Astronomy* 61 (6): 067031. doi: 10.1007/s11433-018-9191-0.

[17] Chen, B. J., Zhao, K., Deng, Z., Han, W., Zhu, J. L., Wang, X. C., et al. 2014. "$(Sr,Na)(Zn,Mn)_2As_2$: A New Diluted Ferromagnetic Semiconductor with The Hexagonal $CaAl_2Si_2$ Type Structure." *Phys. Rev. B* 90 (15): 239906. doi: http://dx.doi.org/10.1103/PhysRevB.90.239906.

[18] Han, W., Chen, B. J., Gu, B., Zhao, G. Q., Yu, S., Wang, X. C., et al. 2023. "Li(Cd,Mn)P: A New Cadmium Based Diluted Ferromagnetic Semiconductor with Independent Spin & Charge Doping." *Scientific Reports* 9: 7490. doi: 10.1038/s41598-019-43754-x.

[19] Li, L. X., Feng, S., Chen, H. Z., and Zhang, L. 2017. "First-Principle Study on the Electronic Structure and Optical Properties of New Diluted Magnetic Semiconductor $(La_{0.75}Ba_{0.25})(Ag_{0.75}Mn_{0.25})SO$." *Journal of Functional Materials* 48 (12): 12177-81. doi: CNKI:SUN:GNCL.0.2017-12-032.

[20] Liu, X. U., Riney, L., Guerra, J., Powers, W., Wang, J., Furdyna, J. K., and Assaf, B. A. 2022. "Colossal Negative Magnetoresistance from Hopping in Insulating Ferromagnetic Semiconductors." *Journal of Semiconductors* 43 (11): 44-53.

[21] Xu, Q., Yang, G. M., and Xing, G. Z. 2015. "Microstructure and Electromagnetism Properties of MnTe and CrTe Diluted Magnetic Semiconductor." *Journal of Jilin University (Science Edition)* 53 (3): 553-60.

[22] Feng, S. 2017. "$Y_{1-x}Sr_xCu_{1-y}Mn_ySO$ First-principles Calculations and Experimental Studies of the Electronic Structure and Optical Properties of the $Y_{1-x}Sr_xCu_{1-y}Mn_ySO$ System." M.Sc. thesis, China Jiliang University.

[23] Feng, S., Chen, H. Z., Li, L.X., and Zhang, L. 2017. "First-Principle Study of the New Diluted Magnetic Semiconductor Parent YCuSO." *Journal of China University of Metrology* 28 (3): 399-403. doi: 10.3969/j.issn.2096-2835.2017.03.021.